Photoinitiated H- and D-atom reactions with N_2O in the gas phase and in N_2O–HI and N_2O–DI complexes

E. Böhmer, S. K. Shin,[a] Y. Chen,[b] and C. Wittig
Department of Chemistry, University of Southern California, Los Angeles, California 90089-0482

(Received 26 March 1992; accepted 8 May 1992)

Reactions of H atoms with N_2O have two product channels yielding NH + NO and OH + N_2. Both channels were observed via NH $A\,^3\Pi \leftarrow X\,^3\Sigma$ and OH $A\,^2\Sigma \leftarrow X\,^2\Pi$ laser-induced fluorescence spectra. Photoinitiated reactions with N_2O–HI complexes yield a much lower [NH]/[OH] ratio than under the corresponding bulk conditions at the same photolysis wavelength. For hot D-atom reactions with N_2O, this effect is somewhat more pronounced. These results can be interpreted in terms of entrance channel geometric specificity, namely, biasing hydrogen attack toward the oxygen. Another striking observation is that the OH and OD rotational level distributions (RLD) obtained under bulk conditions differ markedly from those obtained under complexed conditions, while the NH as well as the ND RLD are similar for the two environments. In addition, OH Doppler profiles change considerably in going from bulk to complexed conditions, while such an effect is not observed for NH. The changes observed with the OH RLD are most likely due to OH–halogen interactions and/or entrance channel specificity. Under bulk conditions, the Doppler shift measurements indicate a large amount of N_2 internal excitation (i.e., $\sim$25 000 cm^{-1}) for the OH ($v = 0$) levels monitored. This is consistent with a reaction mechanism involving an $HNNO^\dagger$ intermediate. The hot hydrogen atom first attaches to the terminal nitrogen of N_2O and forms an excited $HNNO^\dagger$ intermediate having a relatively elongated N–N bond compared with N_2O. Then the H atom migrates from nitrogen to oxygen and exits to the N_2 + OH product channel, leaving N_2 vibrationally excited. A simple Franck–Condon model can reconcile quantitatively the large amount of N_2 vibrational excitation.

I. INTRODUCTION

It is widely acknowledged that the relative orientations, alignments and velocities of approaching reactants play important roles in elementary chemical reaction dynamics in the gas phase. These entrance-channel parameters can determine reaction pathways on the potential-energy surface (PES) and influence overall cross sections, branching ratios, and product state distributions.[1–18] Our research on controlling entrance-channel geometric properties, such as incident angles and impact parameters, has used weakly bonded complexes in order to study photoinitiated reactions with well-characterized initial conditions.[19–38] Namely, the anisotropic intermolecular force field binding the complex results in a stereospecifically aligned precursor.[37] In contrast to most gaseous collision environments, where there is no control over angles and impact parameters, such precursor geometry limited (PGL), reactions offer a novel means of investigating steric effects. In addition, photoinitiation provides a control of the reaction energy by varying the photolysis wavelength, as well as setting the "zero time" of the reaction by using a short laser pulse.[39]

In this paper, data are presented for reactions of hot H and D atoms with N_2O using N_2O–HI(DI) complexes as precursors, as well as the corresponding bulk reactions. Product state distributions are interpreted in terms of the geometries of the weakly bonded precursors, reaction intermediate lifetimes, exothermicities, reverse barrier heights that imprint dynamical bias on product state distributions, and possible contributions from termolecular interactions. For the N_2O–HI(DI) system, changes in the branching ratios for chemically distinct product channels between bulk and complexed conditions are reported to elucidate the entrance channel specificity of photoinitiated reactions under complexed conditions.

Reactions of H and D with N_2O have been studied extensively under bulk conditions.[33,34,36–38,40–45] The following channels have been observed in hot H- and D-atom reactions carried out in our lab as well as in reactions of thermal H and D atoms carried out in other labs:[42,45]

[a] Present address: Department of Chemistry, University of California, Santa Barbara, California 93106.
[b] Present address: Department of Chemistry, University of California, Berkeley, California 94720.

 0021-9606/92/162536-12$06.00

$$H + N_2O \rightarrow OH(X\,^2\Pi) + N_2 \qquad \Delta H_{298} = -21\,820\ cm^{-1}, \tag{1a}$$
$$\rightarrow OH(A\,^2\Sigma) + N_2 \qquad \Delta H_{298} = 10\,700\ cm^{-1}, \tag{1b}$$
$$\rightarrow NH(X\,^3\Sigma) + NO \qquad \Delta H_{298} = 12\,350\ cm^{-1}, \tag{1c}$$
$$D + N_2O \rightarrow OD(X\,^2\Pi) + N_2 \qquad \Delta H_{298} = -22\,310\ cm^{-1}, \tag{2a}$$
$$\rightarrow ND(X\,^3\Sigma) + NO \qquad \Delta H_{298} = 11\,190\ cm^{-1}. \tag{2b}$$

H atoms that attack the oxygen side of N_2O face an entrance barrier of $\sim$7000 cm^{-1}, as shown in Fig. 1.[42] Once past this barrier, NN–OH bond cleavage occurs without involvement of a long lived intermediate.[37,38,42] Product rotational level distributions (RLD) will be biased by the large reverse barrier of $\sim$28 800 cm^{-1}.[42] Attack at the terminal nitrogen, once past a barrier which is smaller than that for oxygen-side attack, leads to an intermediate $HNNO^{\dagger}$ which lies lower in energy by $\sim$5300 cm^{-1} than the reactants.[37,38,42] The reaction can proceed either via 1,3-hydrogen migration to yield exothermic products ($OH + N_2$) or via the high exit channel barrier to yield endothermic products ($NH + NO$).[37,38,42] Substituting deuterium for hydrogen might help discern OH formed by direct oxygen-side attack from OH resulting from 1,3 migration. Unfortunately, deuteration will not only retard 1,3 migration kinetically, but also lower the transition-state energy. The latter will probably influence the endothermic $NH + NO$ channel more than the highly exothermic $OH + N_2$ channel. Doppler shift measurements of $OH(v = 0)$ performed under bulk conditions suggest a very high degree of N_2 internal excitation, presumably vibrational. This offers a clear view of the role of migration. The large amount of N_2 vibrational excitation is most likely the consequence of an $HNNO^{\dagger}$ intermediate whose long N–N bond length is projected onto the vibrations of the N_2 product formed from 1,3-hydrogen migration. A simple Franck–Condon model is used to rationalize the data.

In going from the isotropic environment of bulk $H + N_2O$ collisions to PGL conditions in weakly bonded N_2O–HI complexes, there may be significant changes in the reaction paths. H-atom attack in "inertially T-shaped" N_2O–HI complexes involves entrance channels in which H atoms attack the oxygen and/or nitrogen side. Although the N_2O–HI structure has not yet been determined spectroscopically, it can be inferred from the N_2O–HX (X = F, Cl, Br) systems, which have been studied extensively.[37,38,46] For N_2O–HBr, the average separation between the N_2O and HBr centers of mass, is $R_{c.m.} = 3.64$ Å and the average angle between $R_{c.m.}$ and the N_2O axis is 75–80° (see Table I).[46] In all N_2O–HX complexes studied to date, the H atom is thought to be bonded more strongly to the oxygen than to the terminal nitrogen.[37,38,46] The H atom disfavors the central nitrogen. The observed variation in product branching ratios in going from bulk to complexed conditions is also consistent with preferred localization toward the oxygen side.[37,38] However, we emphasize that even with N_2O–HBr, the localization of the hydrogen atom has not been determined experimentally, and the position shown in Fig. 2 is an educated guess.

It is unlikely that a linear counterpart of FH–NNO exists for HBr or HI, but there are other possibilities besides the one shown in Fig. 2.[37,38,46] Moreover, the halogen atom may participate in the photoinitiated reactions via one or more radical–radical type interactions (e.g., X–OH, X–N(H)NO, X–NO). The aforementioned caveats notwithstanding, D→H substitution can yield useful information, e.g., with a reduced bending amplitude for D in the N_2O–DI

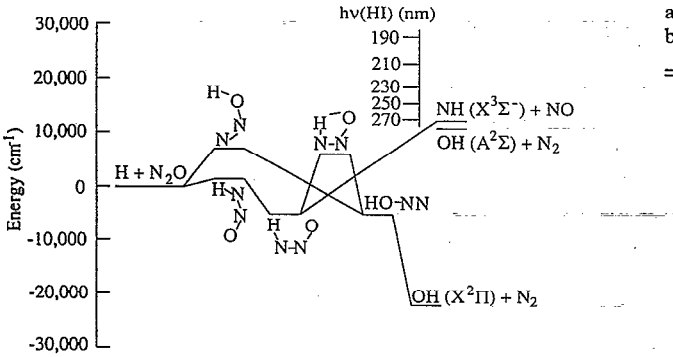

FIG. 1. Energy diagram for the $H + N_2O$ system (Ref. 45). The listed center-of-mass collision energies corresponding to different HI photolysis wavelengths are for the $H + I(^2P_{3/2})$ channel only.

TABLE I. Molecular constants and structural parameters for N_2O–HBr, exciting the N_2O chromophore. Spectra were analyzed using a rigid rotor Hamiltonian of the form $\{(B + C)J^2 + [A - (B + C)/2]J_a^2 + (B - C)(J_b^2 - J_c^2)\}/2$ (Ref. 46), where ν_0 is the observed vibrational band origin. $\Delta\nu$ is defined as ν_0 (complex) $- \nu_0(N_2O)$, with $\nu_0(N_2O) = 2223.756\,91\ cm^{-1}$. The structural parameter $R_{c.m.}$ is the average separation between the N_2O and HBr centers of mass and θ_1 is the angle between $R_{c.m.}$ and the N_2O internuclear axis.

A'' (MHz)	12873.0(34)
B'' (MHz)	1351.3(5)
C'' (MHz)	1220.9(5)
A'' (amu Å^2)	2.62
A' (MHz)	12664.4(35)
B' (MHz)	1368.3(7)
C' (MHz)	1208.8(7)
A' (amu Å^2)	8.81
ν_0 (cm^{-1})	2225.62161(12)
$\Delta\nu$ (cm^{-1})	+1.86
$R_{c.m.}$ (Å)	3.619 ($v = 0$)
	3.638 ($v = 1$)
θ_1 (deg)	75.0 – 81.5 ($v = 0$)
	75.9 – 83.1 ($v = 1$)

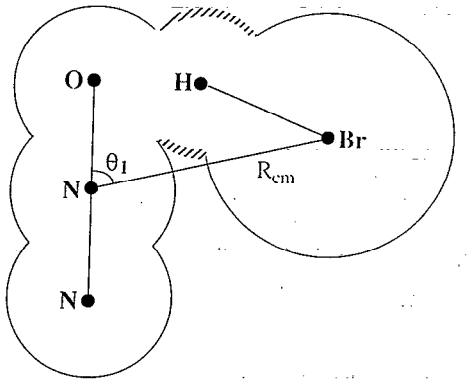

FIG. 2. Structure of the N_2O–HBr complex, showing experimental $R_{c.m.}$ and θ_1 values (Ref. 46). All distances and angles are averaged over the vibrational ground state. Note that the hydrogen position shown is an educated guess.

system, the influence of a preferred O-side attack might be even more pronounced.

The results presented later indicate that under bulk conditions the reaction proceeds mainly via an energized $HNNO^{\dagger}$ intermediate. With complexes, however, there are significant differences. The NH + NO channel is diminished markedly relative to the bulk, and OH RLD are colder as well. This is consistent with preferential H-atom attack at the oxygen side with complexes, although it doesn't prove the point. Results obtained with deuterium substitution are consistent with the aforementioned. Thus, this system also shows that the photochemistry can be quite different with complexed materials relative to the corresponding bulk conditions.[47]

II. EXPERIMENTAL ARRANGEMENT

A schematic view of the experiment is given in Fig. 3. Bulk reactions were initiated in flowing samples of typically 20%–30% HI(DI) and 70%–80% N_2O at 40 mTorr total pressure. N_2O–HI(DI) complexes were prepared by expanding mixtures of ~3% HI(DI), 7%–12% N_2O, and 85%–90% He through a pulsed slit nozzle into a vacuum chamber. The $40\times40\times30$ cm^3 chamber was pumped by a diffusion pump (Varian VHS-10) equipped with a water cooled baffle. The nozzle was based on a piezoelectric disc translator (P-286.27, Physik-Instrumente GmbH). The best signal-to-noise ratios for laser-induced fluorescence (LIF) spectra were obtained by using a 0.25 mm×1 mm nozzle, a backing pressure of ~1500 Torr, and a gas pulse duration of 380–420 μs. The nozzle effluent was monitored 35 cm from the orifice using a quadrupole mass spectrometer (UTI 100C), which was mounted diametrically across from the nozzle in a separate chamber pumped by a liquid-nitrogen trapped pump (Edwards, Diffstak 100). During experiments, the stagnation pressure in the nozzle chamber was ~1–2×10^{-5} Torr, while the pressure in the quadrupole region was $\sim10^{-7}$ Torr. Although care was taken to minimize higher-order clusters, the $(N_2O)_2HI^+$ signal was typically ~10% of the N_2O–HI^+ signal. Contributions from higher-than-binary clusters are therefore present, but are not believed to change the conclusions reported here.

The photolysis and probe beams were collinear and counterpropagating, intersecting the expansion 2.5 cm downstream from the nozzle. Photolysis between 240 and 266 nm was achieved with the doubled output from an excimer-pumped dye laser. Photodissociation yields both ground-state $I(^2P_{3/2})$ and excited-state $I(^2P_{1/2})$. Thus, H(D) atoms are prepared with two different kinetic ener-

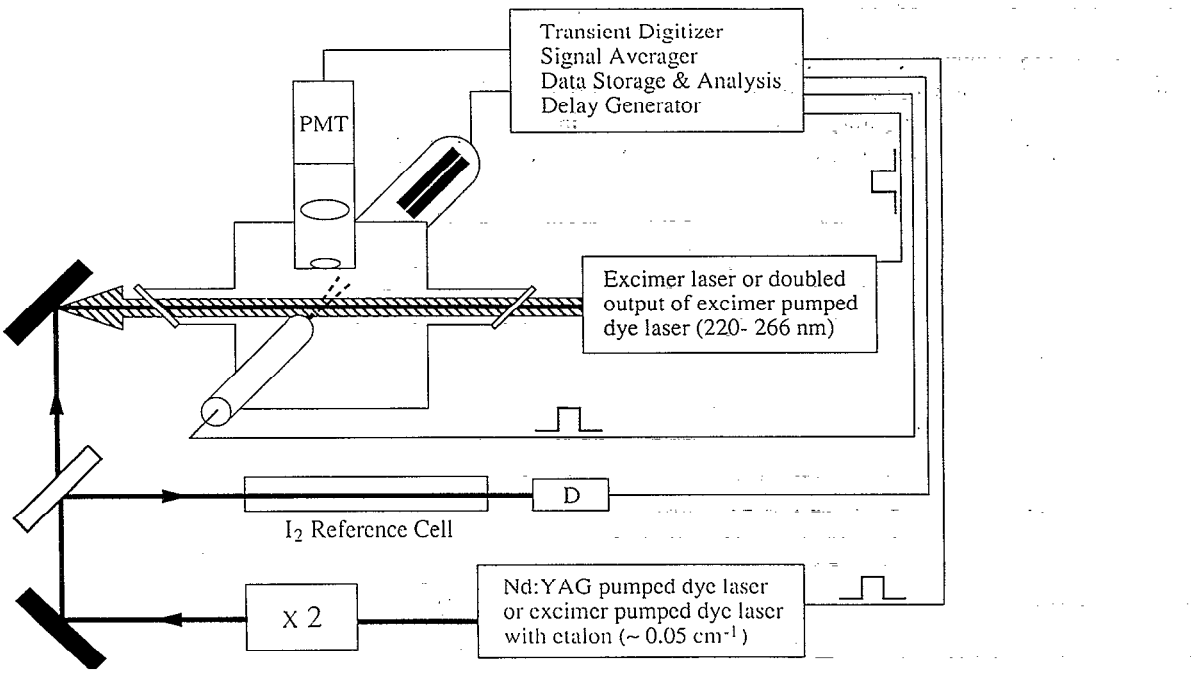

FIG. 3. Schematic view of the experimental arrangement. The I_2 reference cell is used for *in situ* frequency calibration during the sub-Doppler resolution etalon scans.

gies. For 240–266 nm photolysis, the H and D kinetic energies corresponding to $I(^2P_{1/2})$ are insufficient to produce NH or ND. However, contributions to OH and OD production from both faster and slower H atoms have been observed. Figure 4 shows the OH LIF intensity as a function of total available energy under bulk conditions. The observed OH LIF intensity varies linearly with the HI absorption coefficient which reflects the combined contribution of both faster and slower H atoms. The reported OH and OD RLD reflect contributions from both H atoms for all photolysis wavelengths.

Reaction products of hot H and D atoms with gaseous N_2O were probed 100 and 70 ns after photolysis for bulk and complexed conditions, respectively, using a YAG-pumped dye laser (Quanta Ray PDL-1 and DCR I, DCM, and DCM/Kiton Red dyes optimized for 660–680 and 614–630 nm, respectively). To prevent saturation, beam diameters $\geqslant 0.5\ cm^2$ were used at energies ~ 1-$3\ \mu J$; tests for saturation were performed routinely. A 2 m focal length lens located 1.5 m from the detection region brought the photolysis beam diameter to a similar size. Under bulk conditions with 10 ns delay, nascent H atoms undergo ~ 0.3 hard-sphere collisions on average and nascent products undergo < 0.1 collisions on average. Changing either the delay time or the total pressure by a factor of 2 did not affect the product distributions.

III. RESULTS

NH(ND) $A\,^3\Pi \leftarrow X\,^3\Sigma$ and OH(OD) $A\,^2\Sigma \leftarrow X\,^2\Pi$ LIF spectra obtained for bulk and complexed conditions were normalized for laser intensities, pressure (bulk conditions), and mass spectrometer signals (complexed conditions). ND rotational line strengths were calculated according to Kovacs[48] using known ND spectroscopic constants.[49–52] In a complete theoretical description, each vibronic band has 27 rotational branches, of which 9 are main branches with $\Delta N = \Delta J = 0$ and ± 1. ND ($A\,^3\Pi$) belongs to Hund's case (a) for low J and Hund's case (b) for high J, and the remaining 18 satellite branches are weak following the case (a) to case (b) transition. Thus, interference from satellite transitions is low. Typical ND LIF spectra taken under complexed and bulk conditions are shown in Fig. 5. Spectra calculated from published line positions and line strengths,[49–56] convoluted with the experimentally measured line shape, were fitted to the normalized spectra. Rotational distributions for NH(ND) and OH(OD) in $v = 0$, 1 were obtained from satisfactory fits.

Although the (1,1) and (0,0) NH(D) vibronic bands overlap, some lines were resolved well enough for analyses of both bands. Variations of the NH $v = 0$ and 1 concentrations with the photolysis wavelength are presented in Fig. 6 for bulk conditions, showing a cutoff near the thermodynamic thresholds. Below 250 nm, both NH and ND are produced in $v = 1$. Under complexed conditions, NH(D) in $v = 1$ was

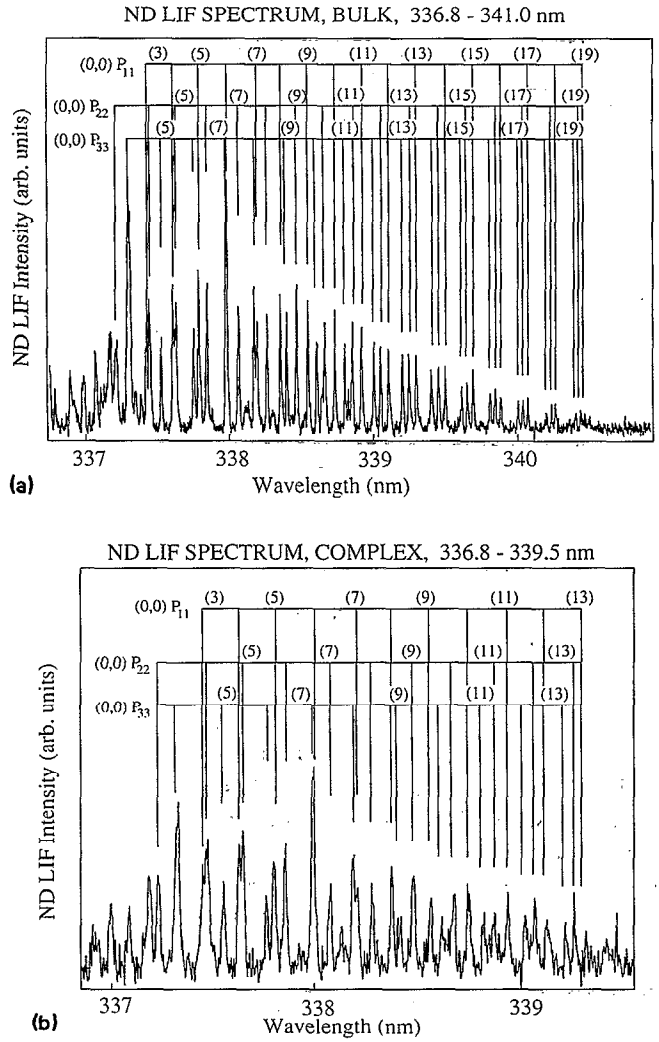

FIG. 5. ND $A\,^3\Pi \leftarrow X\,^3\Sigma$ LIF spectra taken under (a) bulk and (b) complexed conditions on the same day. DI was photolyzed at 240 nm. Only the $A\,^3\Pi \leftarrow X\,^3\Sigma(0,0)$ assignment is shown.

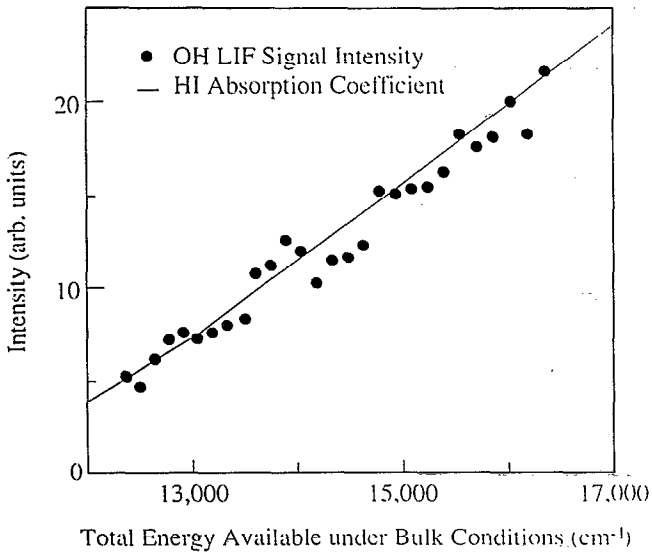

FIG. 4. OH LIF signal intensity is given as a function of total available energy under bulk conditions (i.e., as a function of photolysis wavelength). HI dissociates to $H + I(^2P_{1/2})$ and $H + I(^2P_{3/2})$. The absorption coefficient for HI is indicated by the solid line.

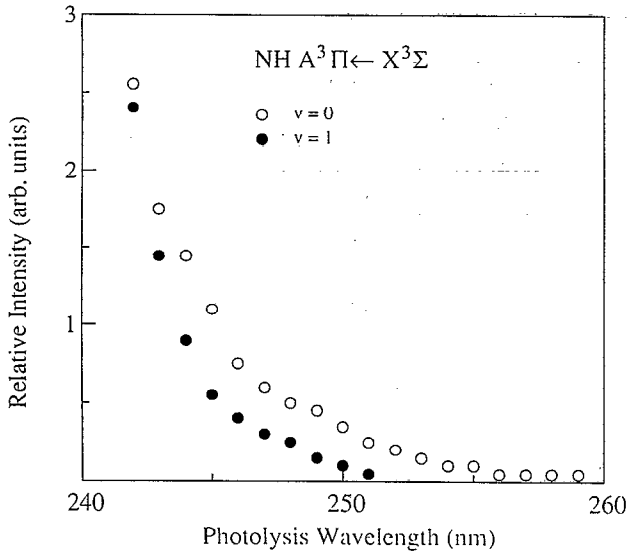

FIG. 6. NH $v = 0$ and 1 relative LIF signal intensities under bulk conditions as a function of photolysis wavelength, showing a cutoff at the thermodynamic threshold.

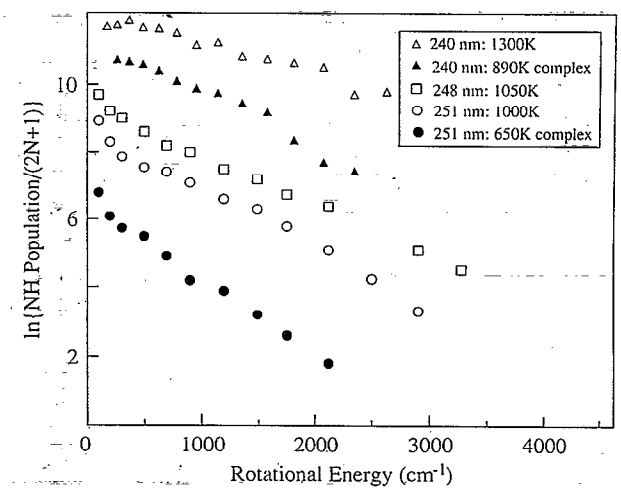

FIG. 8. Logarithmic plots showing NH RLD under complexed and bulk conditions as a function of rotational energy for photolysis in the range 240–251 nm. The data can be fit to straight lines. The solid circles and triangles are for complexed conditions; the others are for bulk conditions. Rotational temperatures are listed in the legend.

not observed. Figure 7 shows ND RLD for both $v = 0$ and $v = 1$ at a photolysis wavelength of 240 nm.

The observed NH and ND RLD can be ascribed temperatures for photolysis wavelengths throughout the range 240–266 nm, as shown in Figs. 8 and 9. These temperatures vary linearly with values of the excess energy, extrapolating to zero at excess energies ~ 0, assuming $\Delta H_0 = 12\,100$ cm^{-1}.[57–59] Referring to the horizontal axis in Fig. 9, the excess energy under bulk conditions is given by the formula

$$E_{\text{excess}} = [127/128]\ [44/45]\ [h\nu - D_0(\text{HI}) + RT] + RT + \langle E_V(N_2O)\rangle - \Delta H_0, \quad (3)$$

which accounts for (i) H-atom motion in the HI c.m. system, (ii) H-atom motion in the $H + N_2O$ c.m. system, (iii) the HI 300 K average rotational energy, and (iv) the N_2O 300 K average vibrational and rotational energies.[37,38] Note that 300 K bulk samples have 410 cm^{-1} of $HI + N_2O$ internal energy which is not present in complexes. In addition, the N_2O–HI binding energy must be overcome.

With N_2O–HI complexes, the NH rotational temperatures are slightly colder than their bulk counterparts at the same photolysis wavelengths. The NH rotational temperatures obtained under complexed conditions can be *placed* on the straight line in Fig. 9, and when this is done the observed

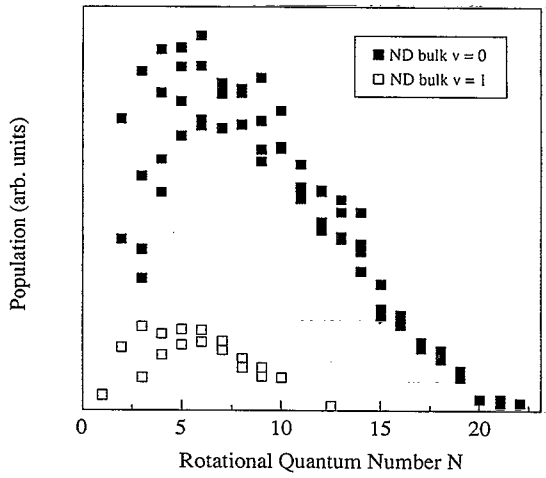

FIG. 7. ND $v = 0$ and 1 rotational distributions under bulk conditions as a *function* of rotational quantum number N. DI was photolyzed at 240 nm. The solid and open squares refer to rotational populations in $v = 0$ and 1, respectively.

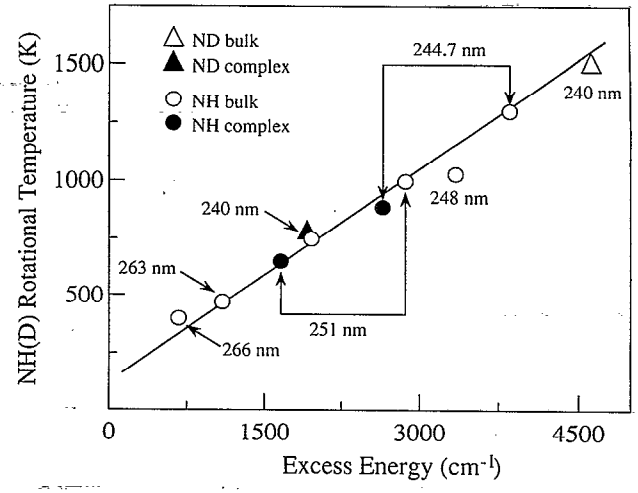

FIG. 9. NH (D) rotational temperature vs excess energy for the bulk reaction. E_{excess} is given by $[127/128]\ [44/45]\ [h\nu - D_0(\text{HI}) + RT] + RT + \langle E_V(N_2O)\rangle - \Delta H_0$. Samples at 300 K contain ~ 470 cm^{-1} of vibrational and rotational energy, while complexes have essentially no internal energy except zero point, and are bound relative to free $N_2O + HI$. Note the difference between NH and ND rotational temperatures under bulk and complexed conditions.

rotational temperatures for photolysis of complexes at 251 and 244.7 nm are the same as for bulk photolysis at 259 and 253 nm, respectively. Thus, with complexes, higher energies are required to achieve the same NH rotational temperatures that would be obtained under bulk conditions (i.e., note the 1200 cm^{-1} differences in Fig. 9).

For the DI/N_2O bulk system, photolysis was carried out at 240 nm so that the c.m. collision energy would match that for HI/N_2O photolyzed at 244.7 nm. The corresponding excess energies favor deuterium by $\sim$800 cm^{-1}, as shown in Fig. 9. The bulk NH and ND RLD are similar enough to suggest that D atoms behave qualitatively in the same way as H atoms. Under complexed conditions, however, the ND rotational temperature is quite a bit lower than for bulk conditions at the same photolysis wavelength. The difference in excess energies is 2700 cm^{-1} as compared to 1200 cm^{-1} for the NH case (see Fig. 9). This may be due to a more efficient squeezed atom effect for deuterium relative to hydrogen.

The OH internal energy is significant, which is not surprising given the considerable amount of energy available for the OH + N_2 channel. Once past an entrance barrier there is no long-lived intermediate and product RLD will be biased by the large reverse barrier. OH internal excitation has been found to be essentially independent of photolysis wavelength in the range 240–270 nm.[35,60] The $[v=1]/[v=0]$ ratio is $\sim$0.5 for the observed rotational levels, i.e., neglecting $v=0$ rotational levels above 8000 cm^{-1}, and for OD this ratio is $\sim$0.6 for bulk and $\sim$0.5 for complexed conditions. Thus, OD has the same qualitative character as OH (see Figs. 10 and 11).

Under bulk conditions, the highest detectable rotational levels were $N\sim30$ for OD ($v=0$), $N\sim23$ for OD ($v=1$), $N\sim25$ for OH ($v=0$), and $N\sim20$ for OH ($v=1$). Under complexed conditions, levels up to $N\sim28$ were observed for OD($v=0$), $N\sim22$ for OD($v=1$), $N\sim22$ for OH($v=0$), and $N\sim17$ for OH($v=1$). Only rotational transitions for which the signal-to-noise ratio (S/N) was >1 were used for further evaluations. For the Doppler shift measurements, where the signal-to-noise ratio is critical, only levels with S/N$\geqslant$15 were used.

In contrast to NH, OH deriving from complexes is much colder rotationally than its bulk counterpart (Fig. 11). This can be attributed to exit channel interactions with

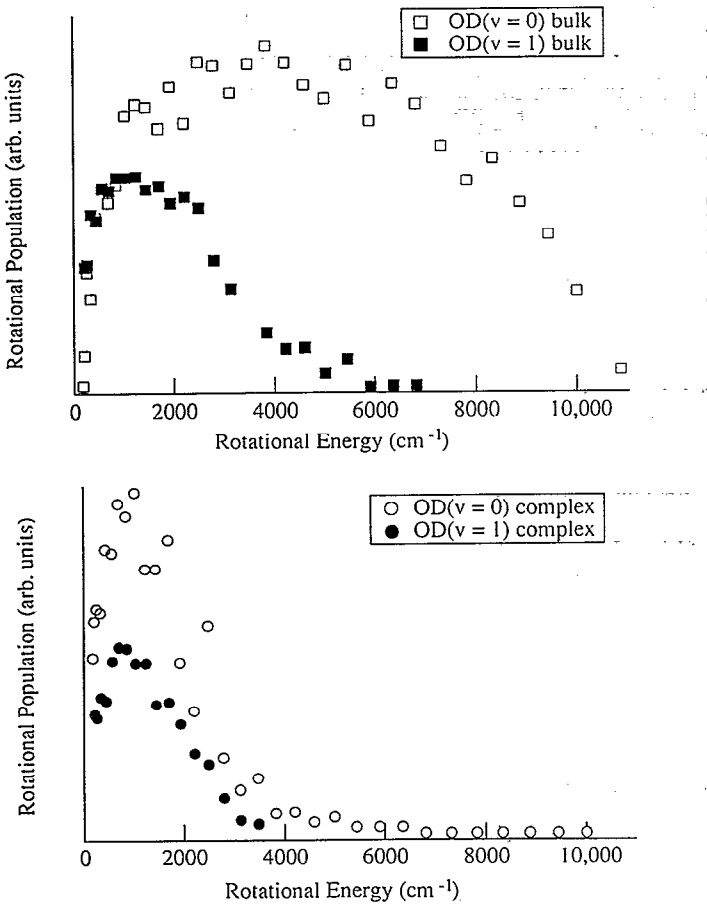

FIG. 10. OD RLD for $v=0$ and 1 under complexed and bulk conditions. DI was photolyzed at 240 nm. The detection of OH($X\,^2\Pi$) by LIF is limited to lower N because of $A\,^2\Sigma$ predissociation. The four RLD are not normalized with respect to one another.

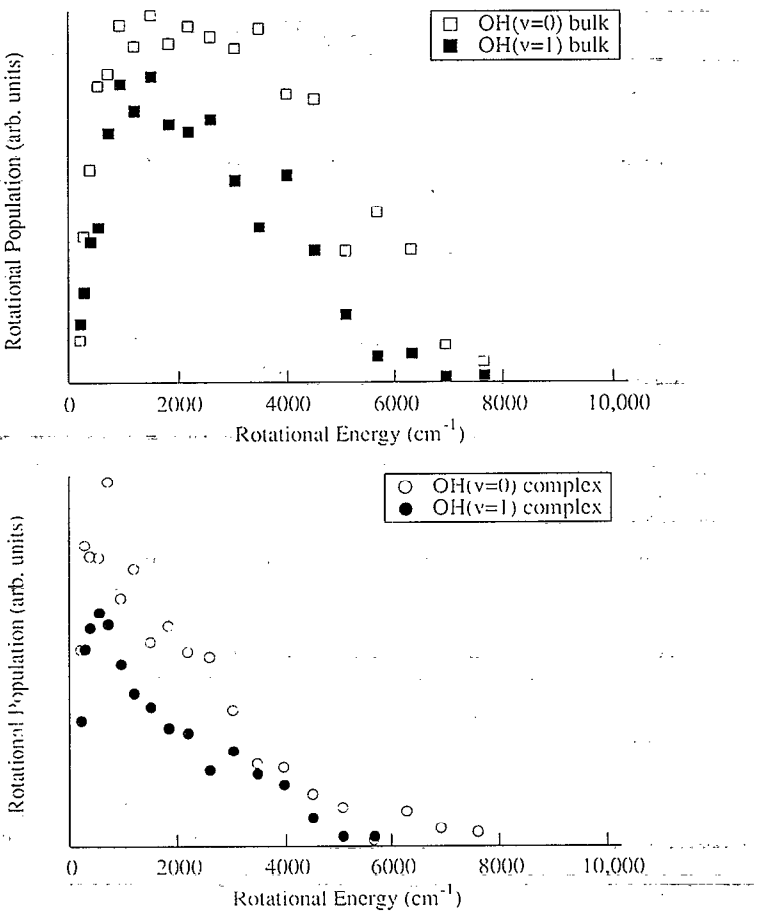

FIG. 11. OH rotational distributions for $v=0$ and 1 under complexed and bulk conditions vs rotational energy. HI was photolyzed at 244.7 nm. Predissociation limits the detection of higher N. Note the shift to lower N in going from bulk to complexed conditions. The $v=0$ and 1 data are not normalized with respect to one another.

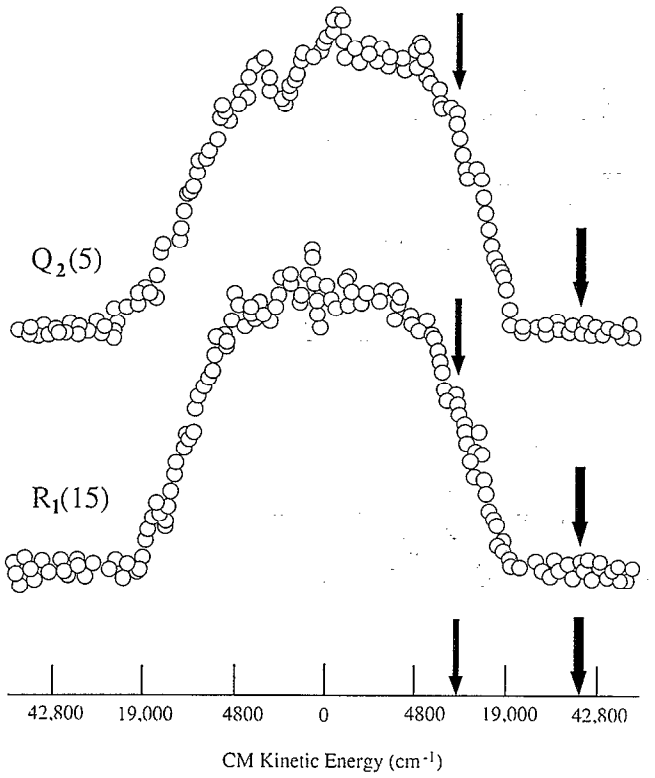

FIG. 12. Sub-Doppler resolution OH LIF spectra from the $H + N_2O \rightarrow OH + N_2$ reaction. HI was photolyzed at 248 nm. The experimental linewidth was ~ 0.05 cm^{-1}. Note the similar line shapes and Doppler widths for $Q_2(5)$ and $R_1(15)$. The line shapes shown are typical of all transitions monitored. The thinner arrows indicate the average c.m. kinetic energy of $\sim 11\,000$ cm^{-1}; the thicker arrows indicate the maximum available energy ($\sim 37\,000$ cm^{-1}).

the nearby I atom,[37,38] as well as different entrance channels under bulk and complexed conditions (e.g., bias toward O-side hydrogen attack with complexes). Therefore, further information about this aspect of the reaction mechanism is needed. It can be obtained by monitoring the translational motion of the fragments. Consequently, $OH(v=0)$ Doppler profiles for the N_2O/HI system were taken under bulk and complexed conditions, using 248 nm photolysis. Delay times were varied between 50 and 300 ns, and Doppler profiles were monitored for the different *P*, *Q*, and *R* rotational branches and for the highest and lowest detectable rotational quantum numbers (3 and 15). No significant changes in line shape or linewidth were observed for any changes of the parameters mentioned earlier. Representative data are shown in Fig. 12.

Under bulk conditions, maximum and mean OH kinetic energies in the c.m. system were $12\,000 \pm 4000$ cm^{-1} and 7000 ± 2000 cm^{-1}, respectively. The uncertainties are liberal. From momentum balance, this corresponds to $19\,300 \pm 6400$ and $11\,300 \pm 3200$ cm^{-1} for the maximum and mean relative kinetic energies in the c.m. system, respectively. This is modest considering that the excess energy is approximately 37 600 cm^{-1}, and that the $OH(v=0)$ levels being monitored have low internal energy, i.e., E_{int} (OH) is typically ~ 1000 cm^{-1} in these measurements. This means that the N_2 fragment is associated with the probed OH levels has an average internal energy $\sim 25\,000$ cm^{-1}. We *assume* that this is mostly vibrational. Although this is a rather remarkable amount of N_2 internal energy, we believe the experimental conclusions to be sound. The data presented in Fig. 12 simply do not support a higher c.m. kinetic energy. This important result will be discussed in Sec. IV within the context of rapid 1,3-hydrogen migration from the nitrogen side to the oxygen side of an $HNNO^{\dagger}$ intermediate that leaves the N–N internuclear separation elongated relative to the diatomic N_2 equilibrium separation. If μ-v correlations are present, they are unlikely to affect the maximum kinetic energies, but might affect the mean c.m. kinetic energies.

Another striking observation is the change in relative NH(D) and OH(D) populations between bulk and complexed conditions. The [NH]/[OH] and [ND]/[OD] ratios for the observed levels drop by factors of ~ 11 and ~ 18, respectively, in going from bulk to complexed conditions (HI and DI were photolyzed at 244.7 and 240 nm, respectively, giving the same collision energies for the corresponding bulk reactions). Both ratios depend on the photolysis energy. This is to be expected, since the OH channel is highly exothermic, while the NH channel is endothermic and its cross section is expected to rise with energy. It should be stressed that the amount of OH and OD presently undetected (i.e., $v \geqslant 2$) might be comparable to the combined $v=0$ and 1 populations. Therefore, OH and OD populations were also estimated by summing vibrational levels up to the energetic limit. Specifically, we used the formula $[v=n]/[v=0] = (0.5)^n [1 + (n-1)^2 \alpha]$, where α is a small constant accounting for anharmonicity.[38(a)] The resulting [NH]/[OH] and [ND]/[OD] ratios are factors of ~ 10 and ~ 14, respectively, higher for bulk than for complexed conditions.

Comparisons of [ND]/[OD] against [NH]/[OH] for bulk and complex conditions showed that [ND]/[OD] > [NH]/[OH] in both environments. Individual changes in concentration of ND and OD compared to OH and NH are not known. For this information absolute concentrations would be needed.

IV. DISCUSSION

The intial conditions of a bimolecular collision can strongly influence its outcome. Different collision energies and orientations can have different reaction probabilities and can yield different product states or even products when more than one chemically distinct channel is available.[28,29,61] When all reactant orientations and impact parameters are allowed, one observes the average effect due to all encounters. However, constrained geometries can lead to high selectivity relative to bulk environments.[28,29,61] Thus, reactions of H atoms with N_2O, in which the anisotropic force field present in the N_2O–HX complex is used to set the stage for entrance channel specificity, is a challenging test case.

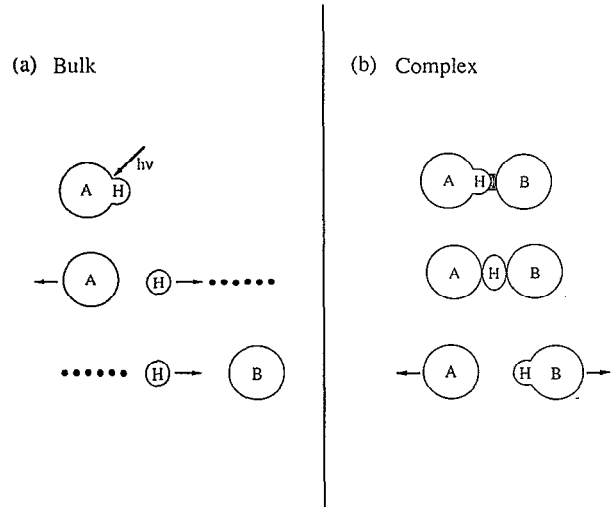

FIG. 13. Schematic drawing indicating the squeezed atom effect. (a) Under bulk conditions AH photodissociation is followed by the formation of a transient intermediate HB, which gives rise to the products (not shown). (b) A weakly bonded AH–B complex is photolyzed. This leads at first to simultaneous AH and BH repulsions that transmit forces to the heavier A and B species until the H atom becomes trapped on the HB potential surface. This results in larger A–HB recoil speed, and correspondingly lower $HB^{\dagger}$ excitation than for case (a).

A. NH(D) internal energies

In comparing experimental results obtained under complexed and bulk conditions, NH(D) rotational level distributions were found to be similar for both cases. The difference in NH(D) rotational energy between the two environments can be rationalized as due, at least in part, to less excess energy available under complexed conditions[47] and to the squeezed atom effect.[32,38,62] The squeezed atom effect has not been observed directly, but is thought to be present in photoinitiated processes involving complexes such as CO_2–HX, RG–HX (RG represents rare gas), N_2O–HX, etc.[28,29,37,61] In an N_2O–HI complex, the H atom is squeezed between its neighbors after photolysis (see Fig. 13) i.e., it is not scattered into a smooth distribution of outgoing continuum states.[37] Although hydrogen is light, it can transmit relative kinetic energy to X and N_2O, resulting in lower $HNNO^{\dagger}$ internal excitation relative to the corresponding bulk experiment,[37] with the halogen carrying away more kinetic energy than under bulk conditions. As a consequence of the squeezed atom effect, $HNNO^{\dagger}$ decomposition will result in diminished product internal excitation.[37]

To see if the NH RLD could be described by statistics, "prior" distributions[15] were calculated and compared with measured distributions for different excess energies. As shown in Fig. 14, the differences between the calculated and measured RLD are largest at low excess energies, the best fit being obtained from 240 nm photolysis, well above reaction threshold. These observations cannot be uniquely reconciled, since there is a competing 1,3-hydrogen migration channel leading to OH + N_2 which might influence the NH RLD.

Although the ND RLD show the same qualitative features as NH RLD under complexed and bulk conditions, the difference between the two environments is larger for ND than for NH, as shown in Fig. 9. For example, 240 nm DI photolysis displays a significant difference between complexed and bulk conditions, with the ND rotational temperature obtained with complexes being the same as for bulk photolysis at 2700 cm^{-1} lower excess energy.

B. OH(OD) excitations

Under bulk conditions, OH $A\,^2\Sigma \rightarrow X\,^2\Pi$ emission was observed as a minor channel in the reaction of H with N_2O. Deactivation of OH($A\,^2\Sigma$) by $N_2(X\,^1\Sigma)$ is thought to be a nonadiabatic process and therefore we believe that surface hopping is most likely responsible for the production of OH($A\,^2\Sigma$).[37,38] Under complexed conditions, no OH($A\,^2\Sigma$) could be detected. This can be attributed to (i) lower excess energy in the complex, (ii) the effect of orientation in the complex, and (iii) quenching due to nearby I.[37,38] In the reaction of D with N_2O, no OD ($A\,^2\Sigma$) was observed under either bulk or complexed conditions. D atoms move more slowly and might not cross efficiently to the surfaces leading to OD($A\,^2\Sigma$) + $N_2(X\,^1\Sigma)$.[15] Since OH($A\,^2\Sigma$) is only a minor channel, it will not be discussed further.

As discussed earlier, OH($X\,^2\Pi$) translational energies were measured from Doppler shifts and the profiles were seen to be insensitive to the levels probed. In addition, OH rotational and vibrational populations did not change over the photolysis wavelength range 263–240 nm. These results suggest bias by the reverse barrier.

C. The role of the $HNNO^{\dagger}$ intermediate under bulk conditions

Under bulk conditions, incident H atoms strike N_2O molecules with all possible angles and impact parameters. They may attach initally to either the oxygen or the terminal nitrogen. We do not think they attach to the central nitrogen, but this is conjecture; isotopic substitution can resolve this. Intuitively, one might think that attachment at the oxygen is most conducive to forming OH. However, this may not be the case. Specifically, *ab initio* calculations of portions of the HNNO potential surface indicate a much lower entrance channel barrier for forming an HNNO intermediate than direct attack at the oxygen to form N_2 + OH.[45] Once HNNO is formed, the barrier for 1,3-hydrogen migration to the oxygen side is narrower and slightly lower than the barrier for direct hydrogen addition at the oxygen side (see Fig. 1). Thus, it is believed that HNNO is the precursor to OH, at least at energies near the barrier heights.[45] Even at higher energies, it may be that the HNNO intermediate is preferred for a democratic set of attack geometries.

The HNNO intermediate may hold the key to understanding the low c.m. kinetic energies and the corresponding high degree of N_2 vibrational excitation. In going from an HNNO intermediate to the NN–OH exit channel, there is a large change in N–N bond length which can promote significant product N_2 vibrational excitation. In order to see how

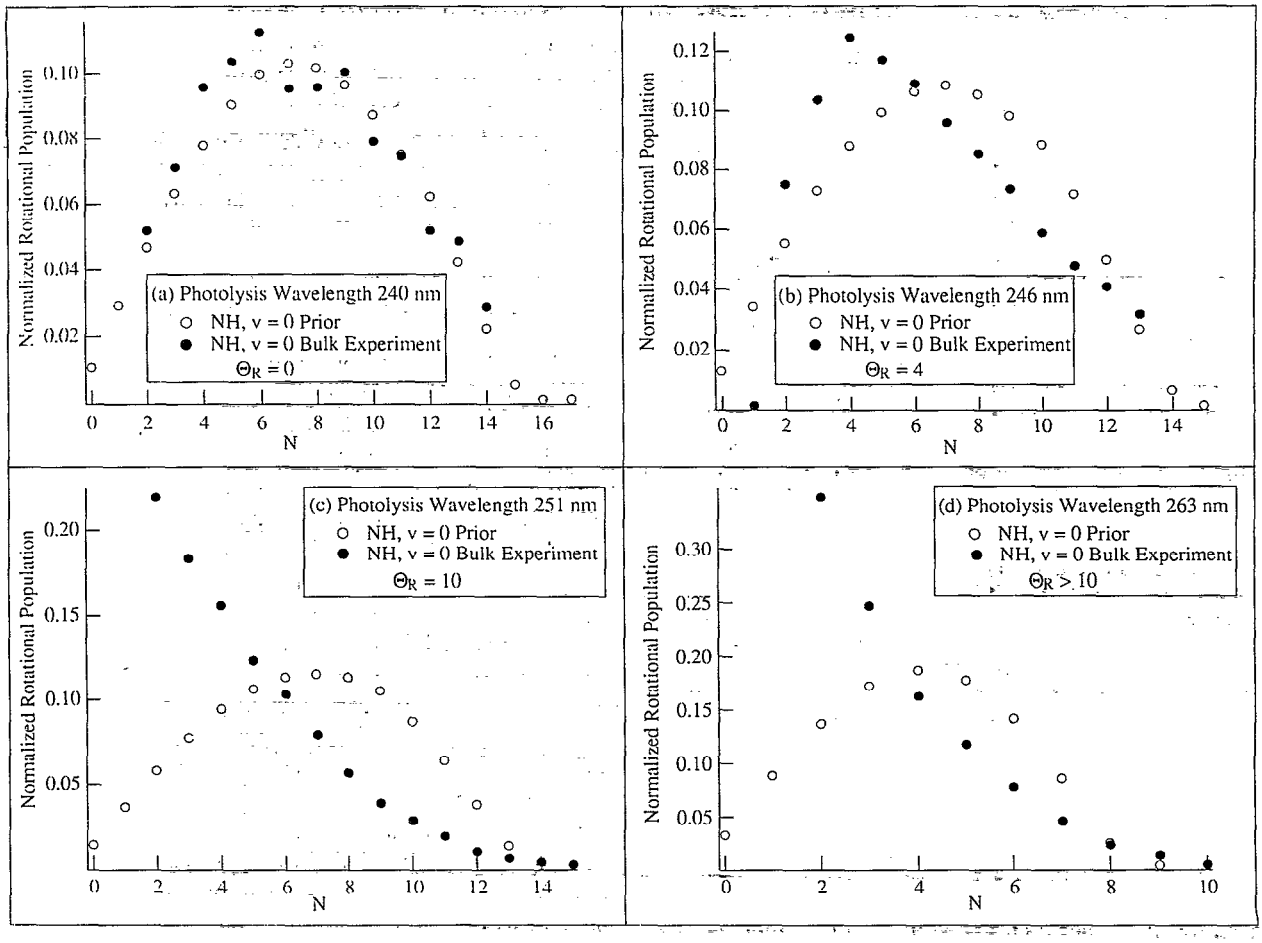

FIG. 14. NH rotational level distributions obtained under bulk conditions (solid circles) for 240, 246, 251, and 263 nm compared to calculated "prior" distributions (open circles). The Θ_R values were obtained from linear surprisal plots (not shown).

large this effect might be, Franck–Condon factors were calculated for projections of the elongated N–N coordinate onto an N_2 vibrational basis. The N_2 vibrations were taken to be harmonic. This calculation is a rough estimate to see if a reasonable mechanism and sensible molecular parameters can reconcile the experimental findings. An implicit assumption is that hydrogen motion is fast enough so that the N–N bond length does not relax appreciably while hydrogen undergoes the 1,3 shift. Note that a hydrogen atom with $\sim 1000\ \mathrm{cm}^{-1}$ of translational energy moves 1 Å in ~ 20 fs.

Figure 15(a) shows the calculated Franck–Condon factors $P_v(N_2) = |\langle \Psi_{N\text{-}N} | v \rangle|^2$, where $|v\rangle$ are harmonic N_2 vibrational wave functions. The wave packet $\Psi_{N\text{-}N}$ is assumed to peak at an N–N separation of 1.23 Å, i.e., the calculated N–N equilibrium separation in HNNO.[45] Gaussian widths near that of free N_2 were used; changes in these widths by $\pm 20\%$ did not lead to different conclusions. Given the crudeness of this estimate, it is not worth exploring the large parameter space of different N–N separations, Gaussian widths, etc. The distribution shown in Fig. 15(a) indicates a high degree of N_2 vibrational excitation, in qualitative agreement with the experimental observations. The average N_2 vibrational enegy from the distribution shown in Fig. 15(a) is $\sim 15\,000\ \mathrm{cm}^{-1}$, which is less than the average N_2 internal energy obtained from the Doppler shift measurements (i.e., $\sim 25\,000\ \mathrm{cm}^{-1}$). However, the $P_v(N_2)$ values do not account for N_2 rotational excitation, which could easily be several thousand cm^{-1}. To take the comparison one step further, we calculated the Doppler spectrum that would be associated with the $P_v(N_2)$ distribution shown in Fig. 15(a), assuming no N_2 rotational excitation and a spatially isotropic distribution of OH velocities. This calculated Doppler spectrum is shown in Fig. 15(b), where it is compared to one of the measured spectra. The agreement is good, lending support to the model.

It is easy to manipulate a better agreement but to some extent this misses the point, namely, that the large amount of N_2 internal excitation observed experimentally can be explained using a chemically intuitive model and a simple back-of-the-envelope calculation. For example, since the HNNO intermediate is highly vibrationally excited, the average N–N distance will be longer than at equilibrium. Maybe this longer N–N bond length should be used instead of the 1.23 Å equilibrium value. As shown in Fig. 16, $R_{N\text{-}N} = 1.24$ Å (corresponding to an average N_2 vibrational energy of $17\,000\ \mathrm{cm}^{-1}$) results in an excellent "fit," but at this point we are guessing.

From the qualitative agreement shown in Figs. 15 and

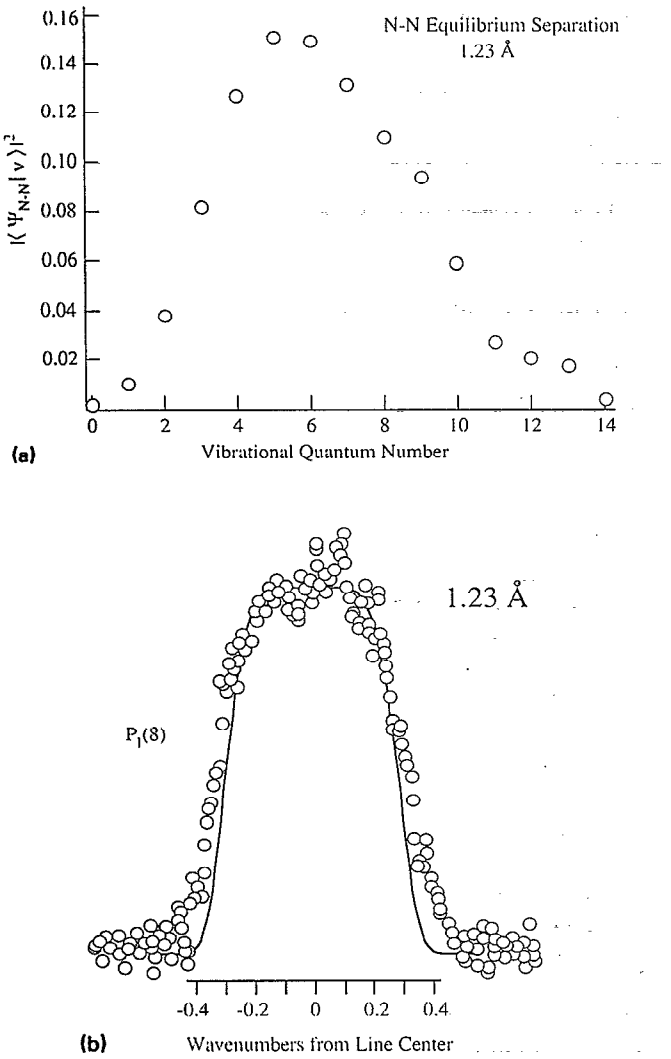

FIG. 15. (a) Calculated Franck–Condon factors $|\langle \Psi_{N-N} | v \rangle|^2$ vs N_2 vibrational quantum number. Ψ_{N-N} is assumed to have a N–N separation of 1.23 Å, i.e., the calculated equilibrium distance in HNNO (Ref. 45). In (b) the experimental Doppler profile is compared to the calculated spectrum for the distribution shown in (a). It is assumed that N_2 rotational excitation is minimal and that the OH velocities are distributed isotropically in the laboratory.

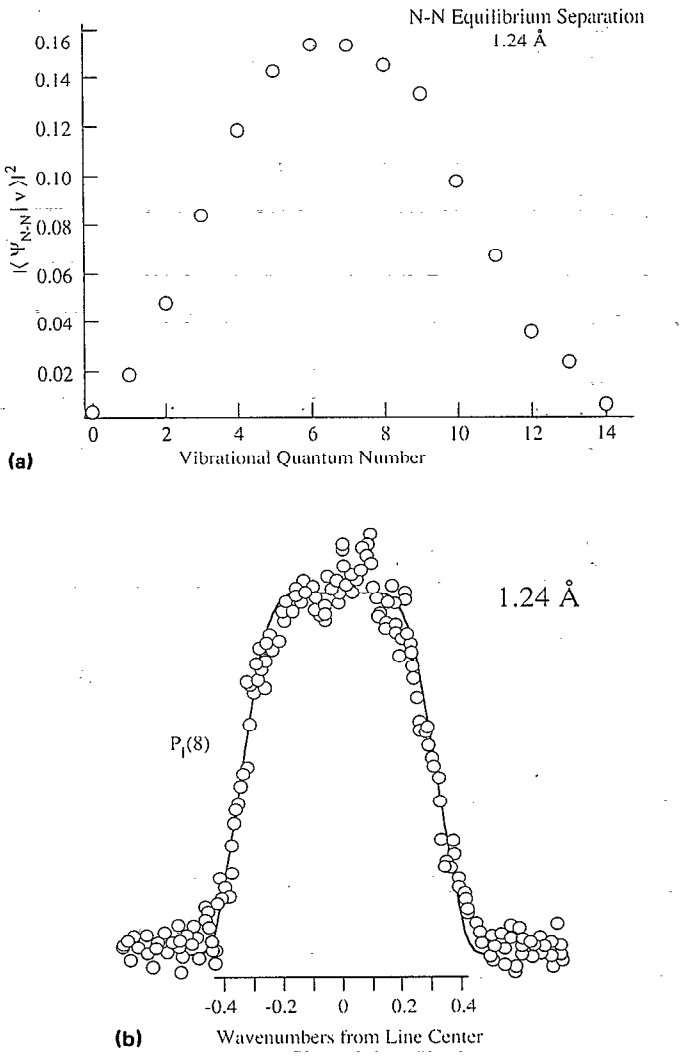

FIG. 16. (a) Calculated Franck–Condon factors $|\langle \Psi_{N-N} | v \rangle|^2$ vs vibrational quantum number. Ψ_{N-N} is assumed to have a N–N separation of 1.24 Å. In (b), the experimental Doppler profile is compared to a calculated spectrum for the distribution shown in (a). It is assumed that N_2 rotational excitation is minimal and that the OH velocities are distributed isotropically in the laboratory.

16, we conclude that, for the OH rotational levels monitored, reaction proceeds predominantly via a vibrationally excited $HNNO^{\dagger}$ intermediate under bulk conditions. We can think of no other way to get a large amount of energy into the N_2 vibrational degree of freedom.

D. Rotational and translational distributions with complexes

Relative to bulk conditions, the OH and OD RLD obtained under complexed conditions are shifted to considerably lower N. Moreover, the Doppler profiles are narrower (Fig. 17) corresponding to less OH translational energy. This has been observed previously in N_2O–HBr,[33–35,37,38,60] and was attributed to HO–X interactions. Detailed information about these interactions is not available, but a possibility is that the halogen forms a short-lived bond with the departing OH, resulting in deactivation. The change in Doppler widths for the N_2O/HI system is less dramatic than for N_2O/HBr.[35,60] Given that the narrower OH Doppler profile under complexed conditions is a strong argument for the presence of HO–X interactions,[35,60] it is tempting to deduce that the interactions with iodine are weaker than those with bromine. NH Doppler profiles do not show such a striking change, although HN–X interactions should be strong, as with HO–X interactions.[44] However, $HNNO^{\dagger}$ may have a sufficiently long decomposition lifetime that the HNNO–X separation is too large at the point of fragmentation for significant HN–X exit channel interactions.

E. [NH]/[OH] and [ND]/[OD] branching ratios

By obtaining NH and OH LIF spectra simultaneously, it was possible to determine the [NH]/[OH] branching ra-

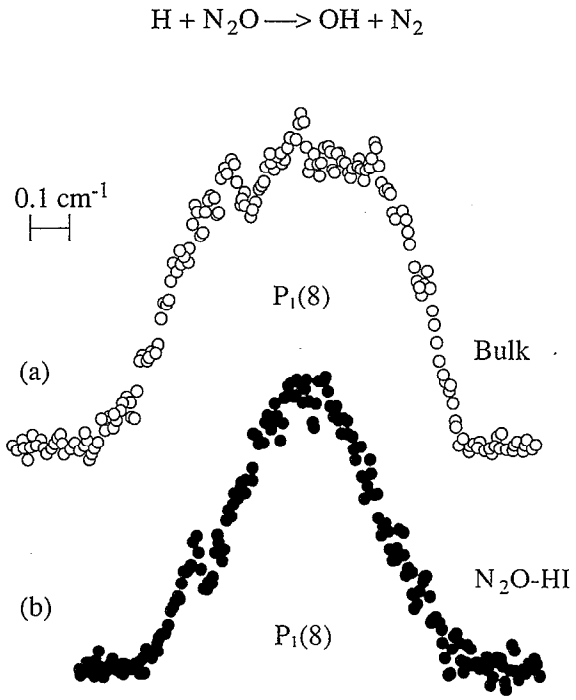

FIG. 17. Sub-Doppler resolution OH LIF spectra from the $H + N_2O \rightarrow OH + N_2$ reaction under bulk and complexed conditions. HI was photolyzed at 248 nm. The experimental linewidth was ~ 0.05 cm^{-1}. Note the different line shapes and Doppler widths for $P_1(8)$ under bulk (open circles) and complexed conditions (solid circles). The maximum relative kinetic energy in the c.m. system changes from $\sim 11\,300$ cm^{-1} to ~ 8100 cm^{-1} going from bulk to complexed conditions, which has been attributed to OH–X interactions (Refs. 33–35, 37, 38, and 60).

tio by comparing the respective signal intensities; the same is true for the deuterated species. Measured signal intensities were corrected for absorption cross sections and fluorescence lifetimes. For NH and ND, summing over the observed internal states was straightforward for bulk and complexed environments. For OH and OD this was not easy. Due to $A\,^2\Sigma$ predissociation, vibrational levels higher than $v = 1$ could not be observed. In addition, high-N states of $v = 0$ and 1 predissociate. Thus, the reported ratios are for the observed $v = 0$ and 1 levels.

Can the observed drop in the [NH]/[OH] and [ND]/[OD] branching ratios be due to a reduction in excess energy alone when going from bulk to complexed conditions? For example, NH RLD obtained for 251 nm photolysis are colder than those obtained under bulk conditions at the same photolysis wavelength. This can be attributed to less excess energy, as evidenced by the fact that the RLD are the same for 251 nm photolysis of complexes and 259 nm of bulk samples. However, a comparison of the [NH]/[OH] ratios obtained at 259 and 251 nm shows that the former is only a factor 3 smaller than the latter. Thus, the observed factor of ~ 11 for N_2O/HI and ~ 18 for N_2O/DI is not due solely to different in excess energies for complexed and bulk conditions.

The above-mentioned arguments assume that the halogen does not participate in the reaction to yield HNI, HOI, INO, etc. Moreover, higher-order complexes must be considered. Although care was taken to minimize their concentrations, they cannot be completely suppressed. We do not believe that the presence of higher-order cluster concentrations that are $\sim 10\%$ of the binary cluster concentration affects the conclusions reported here.

Thus, the observation that the [NH]/[OH] and [ND]/[OD] branching ratios change dramatically in going from bulk to complexed conditions suggests that the H and D atoms might preferentially attack the oxygen side for the cases of complexes. The observed factors of ~ 11 for H and ~ 18 for D cannot be assigned to just lowering the energy, or to the direct dynamical impact of the halogen or to higher clusters, but may be due to dissimilar entrance channels.

V. SUMMARY

Nascent NH and ND from photoinitiated reactions of H and D atoms with N_2O under bulk and complexed conditions have modest rotational and vibrational excitation. The difference between complexed and bulk environments can be attributed to lower excess energies under complexed conditions and to the squeezed atom effect. All NH and ND RLD can be assigned rotational temperatures, but only those obtained at the shortest photolysis wavelengths fit a statistical (prior) distribution. At longer photolysis wavelengths, the observed distributions are colder than the prior distributions.

$OH(A\,^2\Sigma)$ was detected as a minor channel under bulk conditions and was not observed with complexes. $OD(A\,^2\Sigma)$ was not observed at all. $OH(X\,^2\Pi)$ and $OD(X\,^2\Pi)$ rotational excitation was abundant for the highly exoergic $OH + N_2$ channel under bulk conditions, extending to the detection limit of $N \sim 25$. Under complexed conditions, the rotational level distribution in OH and OD shifts dramatically to lower N. This can be attributed to exit channel HO–X interactions and/or a bias toward hydrogen attack of the oxygen under complexed conditions, i.e., a different reaction mechanism.

Under bulk conditions, the Doppler spectra of OH ($v = 0$) indicate an average c.m. kinetic energy of only $\sim 11\,000$ cm^{-1}, compared to $\sim 36\,000$ cm^{-1} of available energy. With only ~ 1000 cm^{-1} of OH ($v = 0$) internal energy in the states being monitored, this leaves $\sim 25\,000$ cm^{-1} of energy in the N_2 internal degrees of freedom, which we assume is mostly vibrational. The effect is very pronounced. There is no possibility that the Doppler spectra can be reconciled with a low degree of N_2 internal excitation. This argues strongly for a reaction mechanism in which an $HNNO^{\dagger}$ intermediate undergoes a 1,3-hydrogen shift to the N_2–OH exit channel. This leaves the N_2 bond elongated, since hydrogen motion is relatively fast. A simple Franck–Condon model can account quantitatively for the large amount of N_2 vibrational excitation.

In going from bulk to complexed conditions, the branching ratio for [NH]/[OH] and [ND]/[OD] is lowered by factors of ~ 11 and ~ 18, respectively. This drop cannot be attributed to lower excess energy under complexed conditions, direct halogen participation on the reaction dynamics, or higher than binary complexes alone.

The data presented so far suggest that under complexed conditions, oxygen side attack may be favored over nitrogen side attack. Taking the spectroscopic data for N_2O–HX (X = F, Cl, Br), together with our experimental findings, it is tempting to conclude that, in N_2O–HI(DI), H(D) atoms that go on to react are localized closer to the O than to the N end of N_2O. However, the location of the hydrogen in the complex awaits further scrutiny. In any event, the precursor limited geometries of H(D)X–N_2O complexes strongly influence the chemistry that follows photoinitiation.

ACKNOWLEDGMENTS

Research was supported by the U.S. Army Research Office Center of Fast Transient Processes and by the U.S. Department of Energy.

[1]K. H. Kramer and R. B. Bernstein, J. Chem. Phys. **42**, 767 (1965).
[2]B. J. Buehler, R. B. Bernstein, and K. H. Kramer, J. Am. Chem. Soc. **88**, 5332 (1966).
[3]R. J. Buehler and R. B. Bernstein, J. Chem. Phys. **51**, 5305 (1969).
[4]A. M. Rulis, B. E. Wilcomb, and R. B. Bernstein, J. Chem. Phys. **60**, 2822 (1974).
[5]D. H. Parker, K. K. Chakravorty, and R. B. Bernstein, J. Phys. Chem. **85**, 466 (1981).
[6]S. R. Ghandi, T. J. Curtiss, Q. X. Xu, S. E. Choi, and R. B. Bernstein, Chem. Phys. Lett. **132**, 6 (1986).
[7]S. R. Ghandi, Q. X. Xu, T. J. Curtiss, and R. B. Bernstein, J. Phys. Chem. **91**, 5437 (1987).
[8]D. van den Ende and S. Stolte, Chem. Phys. Lett. **76**, 13 (1980).
[9]S. Stolte, Ber. Bunsenges. Phys. Chem. **86**, 413 (1982).
[10]S. Stolte, in *Atomic and Molecular Beam Methods*, edited by G. Scoles (Oxford, New York, 1987), Vol. 1, Chap. 25.
[11]D. Parker, H. Jalink, and S. Stolte, J. Phys. Chem. **91**, 5427 (1987).
[12]C. T. Rettner and R. N. Zare, J. Chem. Phys., **77**, 2416 (1982).
[13]R. N. Zare, Ber. Bunsenges. Phys. Chem. **86**, 422 (1982).
[14]M. A. Johnson, J. Allison, and R. N. Zare, J. Chem. Phys. **85**, 5723 (1986).
[15]R. D. Levine and R. D. Bernstein, *Molecular Reaction Dynamics and Chemical Reactivity* (Oxford, New York, 1987).
[16]P. R. Brooks, J. Chem. Phys. **50**, 5031 (1969).
[17]G. Marcelin and P. R. Brooks, J. Am. Chem. Soc. **97**, 1710 (1975).
[18]P. R. Brooks, Science **193**, 1 (1976).
[19]C. Jouvet and B. Soep, Chem. Phys. Lett. **96**, 426 (1983); Laser Chem. **5**, 157 (1984).
[20]W. H. Breckenridge, C. Jouvet, and B. Soep, J. Chem. Phys. **84**, 1443 (1986).
[21]A. Zehnacker, M. C. Duval, C. Jouvet, C. Lardeux-Dedonder, D. Solgade, B. Soep, and O. Benoist-D'Azy, J. Chem. Phys. **86**, 6565 (1987).
[22]C. Jouvet, M. Boivineau, M. C. Duval, and B. Soep, J. Phys. Chem. **91**, 5416 (1987).
[23]M. C. Duval, O. Benoist-D'Azy, W. Breckenridge, C. Jouvet, and B. Soep, J. Chem. Phys. **85**, 6324 (1986).
[24]C. Wittig, S. Sharpe, and R. A. Beaudet, Acc. Chem. Res. **21**, 341 (1988).
[25]M. Hoffmeister, R. Schleysing, and H. L. Loesch, J. Phys. Chem. **91**, 5441 (1989).
[26]S. Buelow, G. Radhakrishnan, J. Catanzarite, and C. Wittig, J. Chem. Phys. **83**, 444 (1985).
[27]S. Buelow, G. Radhakrishnan, and C. Wittig, J. Phys. Chem. **91**, 5409 (1987).
[28]S. Buelow, M. Noble, G. Radhakrishnan, H. Reisler, C. Wittig, and G. Hancock, J. Phys. Chem. **90**, 1015 (1986).
[29]G. Radhakrishnan, S. Buelow, and C. Wittig, J. Chem. Phys. **84**, 727 (1986).
[30]D. Häusler, J. Rice, and C. Wittig, J. Phys. Chem. **91**, 5413 (1987).
[31]J. Rice, G. Hoffmann, and C. Wittig, J. Chem. Phys. **88**, 2841 (1988).
[32]C. Wittig, Y. M. Engel, and R. D. Levine, Chem. Phys. Lett. **153**, 411 (1988).
[33]G. Hoffmann, D. Oh, H. Iams, and C. Wittig, Chem. Phys. Lett. **155**, 356 (1989).
[34]G. Hoffmann, D. Oh, and C. Wittig, J. Chem. Soc. Faraday Trans. **2**, 85 (1989); **2**, 1141 (1989).
[35]Y. Chen, G. Hoffmann, D. Oh, and C. Wittig, Chem. Phys. Lett. **159**, 426 (1989).
[36]G. Hoffmann, D. Oh, Y. Chen, Y. M. Engel, and C. Wittig, Isr. J. Chem. **30**, 115 (1990).
[37]S. K. Shin, Y. Chen, S. Nickolaisen, S. W. Sharpe, R. A. Beaudet, and C. Wittig, Adv. Photochem. **16**, 249 (1991).
[38](a) S. K. Shin, Y. Chen, D. Oh, and C. Wittig, Philos. Trans. R. Soc. London Ser. (A) **332**, 361 (1990); (b) S. K. Shin, Y. Chen, E. Böhmer, and C. Wittig, *Regioselective Photochemistry in Weakly Bonded Complexes*, edited by M. Stuke, Topics in Applied Physics (Springer Verlag, Berlin, 1992), Vol. 70, p. 57.
[39]A. H. Zewail, Science, Wash. **242**, 1645 (1988); A. A. Zewail and R. B. Bernstein, Chem. Eng. News **66**, 24 (1988).
[40]G. Dixon-Lewis and D. J. Williams, in *Gas-Phase Combustion, Comprehensive Chemical Kinetics*, edited by C. H. Bamford and C. F. H. Tipper (Elsevier, Amsterdam, 1977), Vol. 17.
[41]W. E. Hollingworth, J. Subbiah, G. W. Flynn, and R. F. Weston, Jr., J. Chem. Phys. **82**, 2295 (1985).
[42]P. Marshall, T. Ko, and A. Fontijn, J. Phys. Chem. **93**, 1922 (1989).
[43]H. Ohoyama, M. Takayanagi, T. Nishiya, and I. Hanazaki, Chem. Phys. Lett. **162**, 1 (1989).
[44]Y. Chen, G. Hoffmann, S. K. Shin, D. Oh, S. W. Sharpe, Y. P. Zeng, R. A. Beaudet, and C. Wittig, *Advances in Molecular Vibrations and Collision Dynamics*, edited by J. M. Bowman (JAI, City, 1991), p. 187.
[45]P. Marshall, A. Fontijn, and C. F. Melius, J. Chem. Phys. **86**, 5540 (1987).
[46]Y. P. Zeng, S. W. Sharpe, D. Reifschneider, C. Wittig, and R. A. Beaudet, J. Chem. Phys. **93**, 183 (1990).
[47]S. K. Shin, C. Wittig, and W. A. Goddard III, J. Phys. Chem. **95**, 8048 (1991).
[48]I. Kovacs, *Rotational Structure in the Spectra of Diatomic Molecules* (Elsevier, New York, 1969).
[49]M. Shimanouchi, Sci. Light (Tokyo) **15**, 161 (1966).
[50]P. Bollmark, I. Kopp, and B. Rygh, J. Mol. Spectrosc. **34**, 487 (1970).
[51]I. Kopp, M. Kronevist, and N. Åslund, Ark. Fys. **30**, 9 (1965).
[52]D. Patel-Misra, D. G. Sauder, and P. J. Dagdigian, Chem. Phys. Lett. **174**, 113 (1990).
[53]I. L. Chidsey and D. R. Crosley, J. Quant. Spectrosc. Radiat. Trans. **23**, 187 (1980).
[54]R. N. Dixon, Can. J. Phys. **37**, 1171 (1959).
[55]P. W. Fairchild, G. P. Smith, D. R. Crosley, and J. B. Jeffries, Chem. Phys. Lett. **107**, 181 (1984).
[56]W. L. Dimpfl and J. L. Kinsey, J. Quant. Spectrosc. Radiat. Trans. **21**, 233 (1979).
[57]S. T. Gibson, J. P. Greene, and J. Berkowitz, J. Chem. Phys. **83**, 4319 (1985).
[58]K. M. Errin and P. B. Armentrout, J. Chem. Phys. **86**, 2659 (1987).
[59]W. R. Anderson, J. Phys. Chem. **93**, 530 (1989).
[60]Y. Chen, G. Hoffmann, and C. Wittig, J. Chem. Soc. Faraday Trans. II **85**, 1292 (1989).
[61]R. D. Levine and J. L. Kinsey, in *Atom-Molecule Collision Theory*, edited by R. B. Bernstein (Plenum, New York, 1979), p. 693.
[62]R. Alimi, R. B. Gerber, and A. Apkarian, J. Chem. Phys. **89**, 174 (1988).